JACS
JOURNAL OF THE AMERICAN CHEMICAL SOCIETY
Article
pubs.acs.org/JACS

Experimental Demonstration of an Electride as a 2D Material

Daniel L. Druffel,[†] Kaci L. Kuntz,[†,§] Adam H. Woomer,[†,§] Francis M. Alcorn,[†] Jun Hu,[†] Carrie L. Donley,[§] and Scott C. Warren*[,†,§]

[†]Department of Chemistry and [§]Department of Applied Physical Sciences, University of North Carolina at Chapel Hill, Chapel Hill, North Carolina 27599, United States

Supporting Information

ABSTRACT: Because of their loosely bound electrons, electrides offer physical properties useful in chemical synthesis and electronics. For these applications and others, nanosized electrides offer advantages, but to-date no electride has been synthesized as a nanomaterial. We demonstrate experimentally that Ca_2N, a layered electride in which layers of atoms are separated by layers of a 2D electron gas (2DEG), can be exfoliated into two-dimensional (2D) nanosheets using liquid exfoliation. The 2D flakes are stable in a nitrogen atmosphere or in select organic solvents for at least one month. Electron microscopy and elemental analysis reveal that the 2D flakes retain the crystal structure and stoichiometry of the parent 3D Ca_2N. In addition, the 2D flakes exhibit metallic character and an optical response that agrees with DFT calculations. Together these findings suggest that the 2DEG is preserved in the 2D material. With this work, we bring electrides into the nanoregime and experimentally demonstrate a 2D electride, Ca_2N.

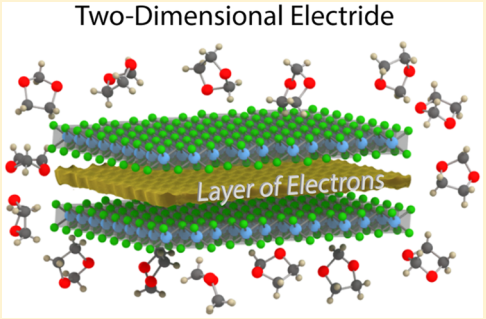

INTRODUCTION

Nearly every ionic solid consists of positively and negatively charged atoms, but in exotic materials called electrides, the negative "ion" is just an electron with no nucleus. The electron's wave function occupies the space typically filled by anions like Cl^-.[1−4] Materials with anionic electrons can serve as strong reducing agents[5,6] or catalysts for chemical syntheses,[7,8] and have been predicted to serve as low-temperature electron emitters,[9] transparent conductors,[10,11] and battery electrodes.[12] With so much to be discovered about electrides, their exotic physical properties may open avenues to different kinds of energy storage,[12] optoelectronic,[13] and magnetic devices.

Electrides have two known structures: cage structures[14−16] in which anionic electrons are located within zero-dimensional cages, and layered structures,[17,18] in which anionic electrons are found in two-dimensional (2D) planes. In layered electrides, the proximity of the anionic electrons causes them to partially delocalize[19] as a 2D electron gas.[18] The electron gas enables high electrical mobility (160 $cm^2\ V^{-1}s^{-1}$ at room temperature),[18] high carrier concentrations ($1.4 \times 10^{22}\ cm^{-3}$),[18] and rapid electrical transport to the material's surfaces.

The exciting properties of layered electrides have prompted theoretical studies into their lower dimensional forms. For example, a recent report[20] presented density functional theory (DFT) calculations of 2D Ca_2N, which suggest that the 2D form could be thermally and mechanically stable and possesses an electron gas on its surface. That result suggests that 2D Ca_2N might be synthesized by exfoliation of 3D Ca_2N. Despite the growing interest, to our knowledge, no electride has been synthesized or experimentally studied as a 2D material or nanomaterial.

Here we demonstrate that electride nanomaterials can be produced by exfoliating a layered electride, Ca_2N. We have applied the liquid exfoliation methodology, previously used to break apart van der Waals solids,[21] to exfoliate the layered Ca_2N crystal into 2D nanosheets. As we show, the 2D flakes are crystalline, have a stoichiometry of $Ca_2N_{0.99\pm0.01}$, and are stable in a nitrogen atmosphere or in several organic solvents for at least one month. In addition, our photoemission and optical measurements, which are consistent with the electronic band structure calculated by density functional theory (DFT), suggest that the anionic electrons are retained in the 2D flakes.

RESULTS AND DISCUSSION

We synthesized bulk Ca_2N by a high-temperature reaction between Ca_3N_2 and calcium metal as reported previously,[18,22] with details described in the Supporting Information, SI. Powder X-ray diffraction patterns of our bulk Ca_2N confirm that the samples have the layered anti-$CdCl_2$-type crystal structure (Figure S1) with lattice parameters matching those in the literature.[17] Figure 1a depicts the crystal structure of Ca_2N, in which planes of Ca_6N octahedra are separated by a 3.9 Å interlayer gap.[17,18,23] Because of the formal oxidation states of Ca^{2+} and N^{3-}, the formula unit has a positive charge and is best represented as $[Ca_2N]^+$. Anionic electrons balance the positive charge of the $[Ca_2N]^+$ layers by occupying the interlayer gap. Using DFT,[24,25] we calculated projections of electron density for the highest occupied band (−1.49 eV to E_F, the Fermi level) shown in Figure 1b (see SI for details). We provide an electron

Received: September 29, 2016
Published: November 16, 2016

DOI: 10.1021/jacs.6b10114
J. Am. Chem. Soc. 2016, 138, 16089−16094

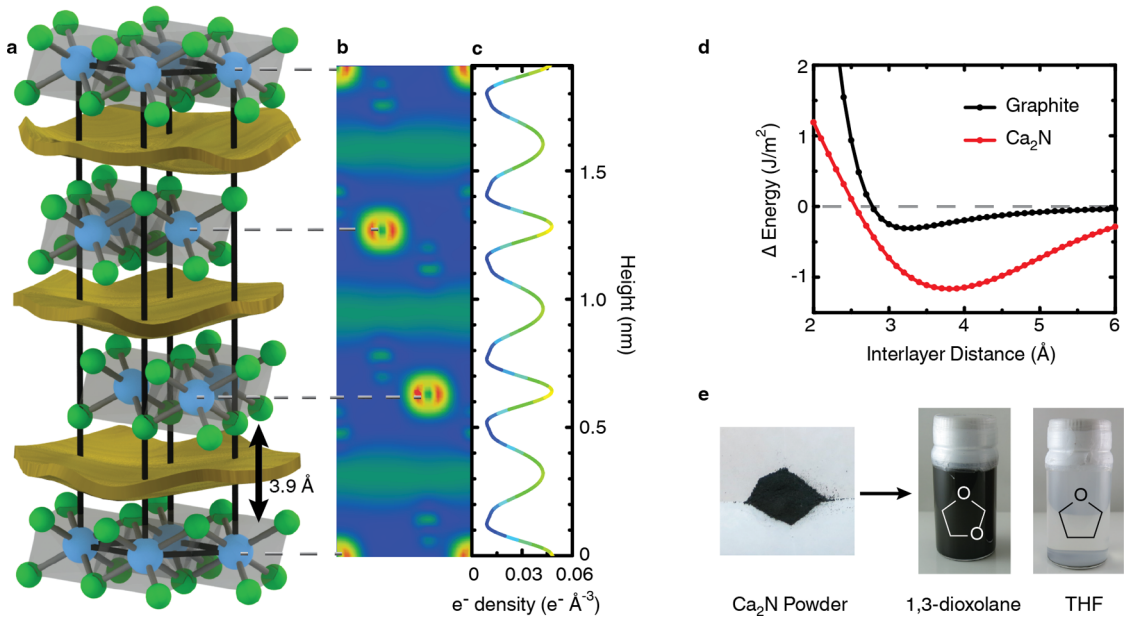

Figure 1. Liquid exfoliation of Ca_2N. (a) The unit cell of Ca_2N depicting layers of $[Ca_2N]^+$ (Ca^{2+} is green, N^{3-} is blue) that alternate with layers of delocalized electrons (gold). (b) Projection of the integrated electron density in the unit cell as calculated by density functional theory (DFT). The integration is over occupied states in the highest occupied band. (c) The electron density profile integrated along the *z*-axis of the unit cell for the occupied band shown in b. (d) Interlayer binding energy versus interlayer distance, as calculated by DFT. (e) Photos of Ca_2N bulk powder and 2D Ca_2N suspensions in 1,3-dioxolane and tetrahydrofuran (THF).

density profile with respect to the *z*-axis of the hexagonal unit cell for this band (Figure 1c) and find that the interlayer electron gas consists of ca. 0.7 electrons per formula unit. The bands below the highest occupied band do not contribute additional electron density to the interlayer electron gas.

To understand the energetics of exfoliating Ca_2N into nanosheets, we calculated the binding energy between layers as a function of interlayer distance. We found that our binding energy between Ca_2N layers was 396 meV per calcium atom or 1.11 J/m^2. These calculations match those performed by others who report a cleavage strength of 1.09 J/m^2 for Ca_2N.[20] In addition, we find that the binding energy of Ca_2N is only about four times that of graphite (0.31 J/m^2), as shown in Figure 1d. Electrostatic interactions between the $[Ca_2N]^+$ and electron gas likely account for the greater binding energy of Ca_2N compared to graphite, a van der Waals solid. These calculations suggest that it may be possible to exfoliate Ca_2N into 2D flakes, although with somewhat greater difficulty than graphite.

Scotch-tape methods used to exfoliate layered van der Waals solids may not be appropriate for Ca_2N. Ca_2N is chemically reactive and can decompose in contact with many adhesives. For such a reactive material, the conditions of liquid exfoliation are more suitable because the solvent's functional groups can be chosen to avoid reaction. Liquid exfoliation offers additional advantages such as a much higher yield, scalability, facile material transfer, and easy thin-film preparation.[21]

To identify solvents that are stable in the presence of Ca_2N, we screened 30 solvents (Table S1) with different functional groups. Working under anhydrous and oxygen-free conditions, we suspended bulk Ca_2N powder in each solvent and sonicated the suspensions for 100 min in a water bath sonicator (see SI for details).

Reactions between many of the solvents and the bulk Ca_2N were easy to identify by eye. As expected, protic solvents like isopropyl alcohol and *N*-methylformamide reacted vigorously with Ca_2N to form $Ca(OH)_2$. In other solvents—chloroalkanes, ketones, aldehydes, nitriles, and even some ethers—the dark blue Ca_2N powder decomposed to a white powder in less than 24 h. Therefore, these solvents are not appropriate for liquid exfoliation. Nonpolar hydrocarbons including benzene and hexanes did not react with Ca_2N, but the dispersions precipitated within minutes. While nonpolar hydrocarbons may not be appropriate for liquid exfoliation, this finding suggests that they could be used to protect Ca_2N from air or water environments. Finally, exfoliation in aprotic amides like *N*-methyl-2-pyrrolidone showed only modest stability: the materials precipitated rapidly and partially oxidized to $Ca(OH)_2$ over a period of 5 to 10 days.

Through the screening process we identified several promising solvents that did not visibly react with Ca_2N, including 1,3-dioxolane, dimethyl carbonate, and dimethoxyethane. These solvents have been successfully employed in lithium-ion batteries[26,27] and are stable against reduction. Although each of these three solvents merits further study, we pursued 1,3-dioxolane because it produced the darkest, most concentrated dispersions and because of its volatility (boiling point = 75 °C).

Although the chemical structures of 1,3-dioxolane, tetrahydrofuran (THF), and 1,4-dioxane are similar, the reactivity of these solvents toward Ca_2N is markedly different. Ca_2N is stable in 1,3-dioxolane for at least a month and remains as a dark suspension, whereas in THF and 1,4-dioxane, it decomposes into white $Ca(OH)_2$ in less than 1 day (Figure 1e, S2). Further studies are underway to better understand the greater stability of Ca_2N in 1,3-dioxolane.

After identifying 1,3-dioxolane as a promising solvent, we sought to characterize the exfoliated material. Figure 2a shows an image of a nanosheet of Ca_2N acquired using a high-resolution transmission electron microscope (HR-TEM). The material is a single crystal and crystalline out to the edges of the flake, which suggests minimal degradation of the sample during the exfoliation process or while loading into the TEM. The

DOI: 10.1021/jacs.6b10114
J. Am. Chem. Soc. 2016, 138, 16089−16094

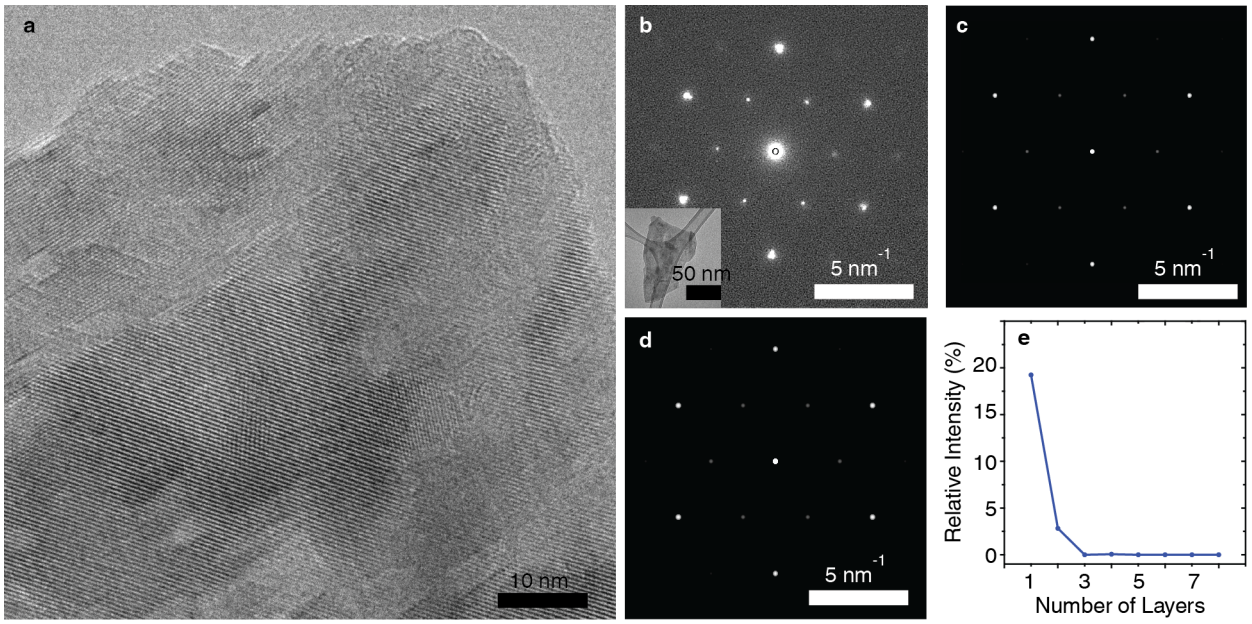

Figure 2. Morphology and crystallinity of exfoliated Ca_2N. (a) High resolution TEM image of 2D Ca_2N showing the sheet-like morphology and crystallinity. (b) Diffraction pattern of 2D Ca_2N with the low resolution TEM image of the corresponding 2D flake. Simulated diffraction pattern of (c) bilayer Ca_2N and (d) Ca_2N with translational disorder looking down the [001] zone axis. (e) Comparison of the relative intensity of the spots at 3.21 nm^{-1} to the spots at 5.56 nm^{-1} in the simulated diffraction patterns for different thicknesses of 2D Ca_2N.

nanosheet is flat and transparent to electrons. Although the predominant morphology is sheet-like, our liquid-exfoliation method does yield some material that is nonsheet-like or that appears to be an aggregate of sheets (Figure S4), despite our attempt to isolate the thinnest materials by centrifugation. We also note that like other liquid exfoliated materials,[21,28,29] our 2D Ca_2N flakes have a distribution of lateral dimensions (approximately 0.2−10 μm) and thicknesses.

We analyzed selected area diffraction patterns to understand the crystal structure of the nanomaterials. The diffraction patterns showed a hexagonal crystal structure with a *d*-spacing of 1.80 ± 0.01 Å, which matches the simulated *d*-spacing (1.80 Å) for the {1,1,0} family of planes. In addition, we observed a second set of hexagonal diffraction spots with a larger *d*-spacing (3.12 ± 0.02 Å) not present in the simulated patterns of bulk Ca_2N.

To understand the origin of the spots with a larger *d*-spacing, we used multislice calculations (JEMS)[30] to simulate diffraction patterns for crystals of differing thicknesses and translational disorder. We found that these spots are present in the diffraction pattern of Ca_2N structures that break the unit cell's symmetry in the *z*-direction. For example, the spots are present in simulated diffraction patterns for monolayer and bilayer structures (Figure 2c,e) as well as structures with translational disorder (Figure 2d, S5, see SI for details).

One possible explanation for the presence of translational disorder is turbostratic disorder either present in the 3D parent crystal or introduced in the exfoliation process by grinding the crystal into a powder or by sonicating the powder into 2D flakes. This possibility fits with recent DFT calculations that show that the energy barrier to laterally slide planes of $[Ca_2N]^+$ in a crystal is remarkably low, only ∼17 meV.[31] Though we have shown that the layer thickness or translational disorder can explain this data, we note that partial oxidation of the sample surface or a surface reconstruction are also possible explanations. Therefore, we conclude that the crystal structure of our 2D Ca_2N is hexagonal with lattice parameters matching the bulk crystal and that there is aperiodicity in the *z*-direction.

To understand the composition of our 2D material, we measured the calcium and nitrogen content of samples of bulk (3D) Ca_2N and exfoliated (2D) Ca_2N. Details of the assays and an experimental confirmation of the applicability of these assays are given in the SI. We measured the stoichiometry of the 3D crystal as $Ca_2N_{1.00\pm0.01}$ and of the 2D material as $Ca_2N_{0.99\pm0.01}$ with the error reported as twice the standard deviation. A two-sample *t* test with a significance level of 0.05 suggests that the compositions of the 3D and 2D material are not different; however, a one-sample *t* test with a significance level of 0.05 suggests that the stoichiometry of the 2D material is nitrogen-deficient or calcium-rich compared to the expected ratio of Ca_2N. This result can be explained by a small amount of oxidation on the surface of the 2D material that resulted in the loss of nitrogen as ammonia gas. Therefore, it is likely that the exfoliated material has slightly oxidized during the exfoliation process or subsequent handling.

X-ray photoelectron spectroscopy (XPS) provides insight into the chemical environment of the surface of our exfoliated Ca_2N. The calcium 2p core electron spectra (Figure 3a, Table 1) of 2D Ca_2N have a Ca 2p doublet with a spin−orbit splitting of 3.5 eV. The Ca $2p_{3/2}$ peak is centered at 347.5 ± 0.2 eV (Table 1) with a full-width-half-max (fwhm) of 1.9 eV. In addition, the Ca 2p spectra show plasmon loss peaks shifted by 7.9 and 11.4 eV relative to the Ca $2p_{3/2}$ center. These values are in agreement with our 3D Ca_2N (Table 1) and with previous literature.[32] After the measurement, we exposed the 2D Ca_2N samples to ambient conditions, which caused oxidation and a corresponding color change from black to white. The XPS spectra of these deliberately oxidized samples match that of $Ca(OH)_2$ (Figure 3a, S6, and Table 1). We conclude that the surface of our as-synthesized 2D Ca_2N has not oxidized to $Ca(OH)_2$. However, because the Ca 2p binding energy is relatively insensitive to the local chemical environment,[33] we do

DOI: 10.1021/jacs.6b10114
J. Am. Chem. Soc. 2016, 138, 16089−16094

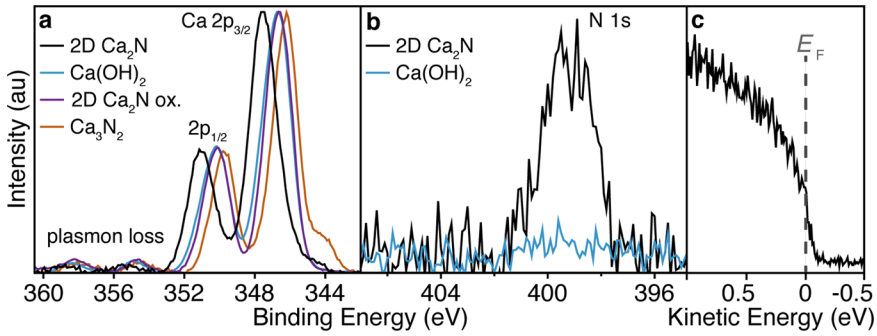

Figure 3. Photoemission spectra of calcium nitride species and related oxidized species. (a) XPS spectra of core Ca 2p electrons for 2D Ca_2N, deliberately oxidized 2D Ca_2N, Ca_3N_2, and $Ca(OH)_2$. (b) XPS spectra of core N 1s electrons for 2D Ca_2N and $Ca(OH)_2$. (c) Ultraviolet photoemission spectroscopy Fermi edge of the metallic 2D Ca_2N.

not draw further conclusions about the surface of our 2D Ca_2N from the Ca 2p peak positions.

Table 1. XPS Binding Energies (eV) of Ca 2p Electrons from Ca_2N

material	$2p_{3/2}$	$2p_{1/2}$	plasm. A	plasm. B
2D Ca_2N	347.5	351.0	355.4	358.9
3D Ca_2N	347.5	351.0	355.5	359.0
Ca_3N_2	346.2	349.7	354.3	358.0
$Ca(OH)_2$	346.7	350.3	354.8	358.3
2D Ca_2N ox.	346.6	350.2	354.7	358.3

To further understand the chemical environment of the surface of our 2D Ca_2N, we examined the nitrogen 1s core electron binding energy (Figure 3b). We attribute the peak, centered at 399.2 ± 0.1 eV with a fwhm of 2.2 eV, to the N 1s core electrons in 2D Ca_2N, in agreement with our 3D Ca_2N (399.3 ± 0.1 eV). We note the N 1s peak is positioned at a different binding energy than previously reported, but we cannot compare absolute positions because a carbon reference was not provided.[32]

The C 1s core electron spectra (Figure S6) show that adventitious carbon species such as adsorbates from 1,3-dioxolane are present on the surface of our 2D Ca_2N. While our measurements are representative of the surface of our liquid exfoliated 2D Ca_2N, future XPS measurements on clean 2D Ca_2N cleaved in vacuum are needed to provide more insight into the intrinsic bonding and local environment of 2D Ca_2N.

Ultraviolet photoelectron spectroscopy (UPS) offers information about the electronic structure of our 2D flakes. The density of states at the Fermi energy, E_F, (Figure 3c) demonstrates that the electronic structure of our 2D Ca_2N is metallic (Figure S7). The work function of our material could not be quantified because all samples of bulk and 2D Ca_2N showed evidence of differential charging (Figure S8 and SI for details), in agreement with previous reports.[32]

In order to better understand the electronic structure of our 2D Ca_2N solutions, we measured the optical response of our 2D flakes with UV−visible−near IR (λ = 280−2200 nm) transmission spectroscopy. Dilute solutions of 2D Ca_2N in 1,3-dioxolane were light brown in color and transparent (Figure 4a), with an optical extinction that depended linearly on sample concentration (Figure S9), which allows us to estimate an attenuation coefficient and molar extinction coefficient (Figure 4b). Concentrated solutions (1.05 mg/mL) appear opaque (inset Figure 4b) and transmit less than 1% of light at certain wavelengths.

UV−visible−near IR spectra of 2D Ca_2N suspensions show absorbance peaks at 330 and 480 nm (Figure 4c). To understand the origin of these peaks, we compare our measurements both to our calculated joint density of states (JDOS), for which we used the OptaDOS code,[34−36] and to previously reported[18] experimental data on 3D Ca_2N. The JDOS shown in Figure 4d (see SI for details), has local maxima at wavelengths of 360 and 560 nm, in agreement with our experimental results. In addition, we extended a previously reported[18] Drude-Lorentz fit of a reflectivity spectrum for 3D Ca_2N to calculate the attenuation coefficient of the 3D material (Figure 4e, see SI for details). We calculated that the 3D material has local maxima at 360 and 520 nm, in agreement with the JDOS and our experimental data of 2D Ca_2N. Therefore, we assign the peaks in the UV−vis spectra of 2D Ca_2N to interband transitions.

We can learn more about the nature of the interband transitions by examining the calculated band structure of 2D Ca_2N (Figure 4f). Projections of the electron density integrated over states with energies −1.50 to −1.72 eV (highlighted in blue in Figure 4f) show that the electron density resides in the N *p* orbitals (Figure 4g), in agreement with previous findings.[19,37] Projections of the electron density integrated over states with energies 0 to +1.00 eV (highlighted in gold in Figure 4f) show that when these states are populated, the electron density occupies the interlayer gap (Figure 4h). Interestingly, direct transitions from the flat band (blue) to the unoccupied conduction band (gold) constitute nearly 100% of the lowest energy transitions, which begin at 900 nm (1.38 eV) to about 700 nm (1.77 eV) (Figure S10). In addition, about 50% of the direct transitions that make up the peak at 560 nm in the JDOS result from transitions from these bands. This suggests that interband absorption events may add electron density to the interstitial electron gas, which could impact the material's work function and electrical conductivity under high intensity illumination.

The near IR data show a response at wavelengths longer than 800 nm (Figure 4b). To qualitatively understand whether the long-wavelength response is dominated by scattering or absorbance, we measured the transmittance with the cuvette inside or outside an integrating sphere (Figure S11). The difference between the spectra, which should be due primarily to light scattering, does not have the same wavelength-dependence as the long-wavelength signal itself. In addition, the attenuation for the two geometries differs by only 20%.

DOI: 10.1021/jacs.6b10114
J. Am. Chem. Soc. 2016, 138, 16089−16094

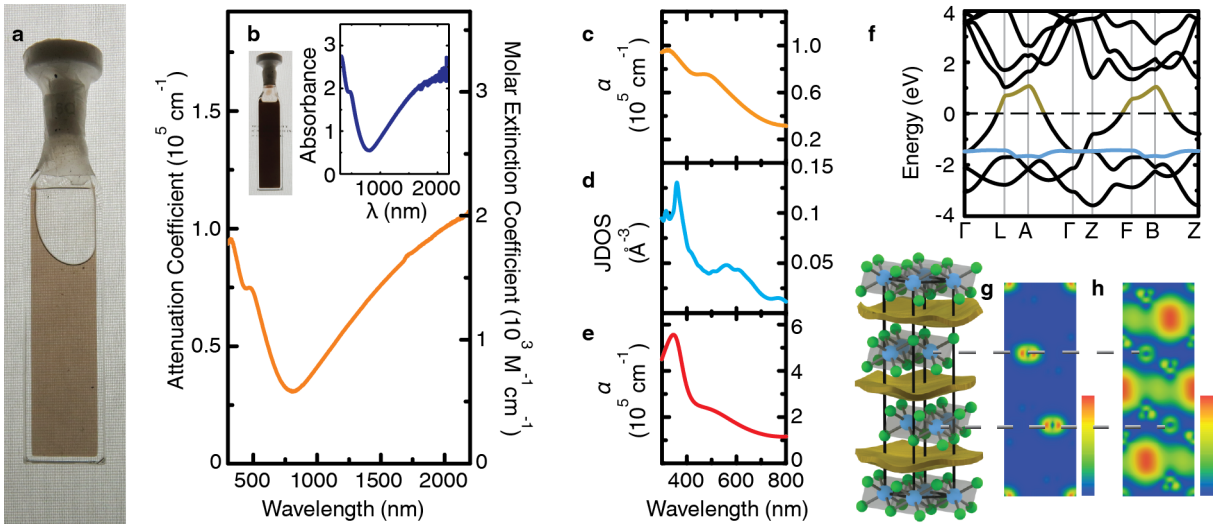

Figure 4. Optical properties of 2D Ca_2N. (a) Photo of a cuvette containing 2D Ca_2N suspended in 1,3-dioxolane. (b) The attenuation coefficient and molar extinction coefficient of 2D Ca_2N vs the wavelength of light. The inset of (b) shows a photo of a cuvette containing concentrated 2D Ca_2N and its absorbance spectrum. The short-wavelength response (300−800 nm) comparing (c) the attenuation coefficient α of 2D Ca_2N, (d) the joint density of states calculated by density functional theory for 2D Ca_2N, (e) the attenuation coefficient α of 3D Ca_2N calculated from literature data.[18] (f) The band structure of Ca_2N. Projection of the integrated electron density in the unit cell integrated over (g) states in the flat band (shown in blue in f) and over states in the band (shown in gold) above the Fermi level. The scale bars for g and h are 0.00 to 1.49×10^{-3} e^- $Å^{-3}$ and 0.00 to 0.12×10^{-3} e^- $Å^{-3}$, respectively.

This suggests that the near IR response is largely due to the absorbance of light and not scattering. The long-wavelength response is most likely the result of an intraband absorbance of the 2D electron gas, although understanding the nature of the response will require samples that are more uniform in size than are produced in this work (see SI for details).

CONCLUSIONS

We have demonstrated that layered electrides can be exfoliated into 2D nanosheets despite the electrostatic interactions that hold the layers together. We have shown that the exfoliated 2D flakes are crystalline and metallic, which suggests that the delocalized anionic electrons are preserved in the 2D system.

This work provides the first demonstration of a conceptually new class of high surface-area, electride nanomaterials. These materials combine the high surface area of 2D materials with the exotic properties of anionic electrons. For example, monolayer Ca_2N has a theoretical specific surface area of 1460 m^2/g, which far exceeds the highest reported specific surface area (~20 m^2/g) of other electrides.[38] At the same time, Ca_2N has a high electrical conductivity (3.57×10^5 S/cm),[18] comparable to Al metal,[39] and a low work function (2.4 to 3.5 eV),[17,40] comparable to alkaline earth metals.[41] The material has high transparency for a metal: our experiments show that a 10 nm thick film would transmit 97% of light, while also having a sheet resistance of just 4 Ω/□. The properties of these electride nanomaterials suggest a number of applications, such as reagents or catalysts in chemical synthesis,[5−8] as transparent conductors,[10,11] or as battery electrodes.[12]

ASSOCIATED CONTENT

Supporting Information

The Supporting Information is available free of charge on the ACS Publications website at DOI: 10.1021/jacs.6b10114.

3D Ca_2N synthesis and characterization, DFT calculations, methods of screening solvents for liquid exfoliation of Ca_2N, transmission electron microscopy and simulations, calcium and nitrogen assays, photoemission, and optical response of 2D Ca_2N (PDF)

AUTHOR INFORMATION

Corresponding Author

*sw@unc.edu

ORCID

Scott C. Warren: 0000-0002-2883-0204

Author Contributions

§These authors contributed equally to this work.

Notes

The authors declare the following competing financial interest(s): We have filed a patent disclosure on the method of synthesis reported herein.

ACKNOWLEDGMENTS

S.C.W. acknowledges support of this research by UNC Chapel Hill startup funds and NSF grants (DMR-1429407 and DMR-161769). A.H.W. acknowledges support of this work by the NSF Graduate Research Fellowship under Grant No. DGE-1144081. This work was performed in part at the Chapel Hill Analytical and Nanofabrication Laboratory, CHANL, a member of the North Carolina Research Triangle Nanotechnology Network, RTNN, which is supported by the National Science Foundation, Grant ECCS-1542015, as part of the National Nanotechnology Coordinated Infrastructure, NNCI. The measurements on the optical response of 2D Ca_2N were performed using a Cary 5000 double-beam spectrometer in the UNC EFRC Instrumentation Facility established by the UNC EFRC Center for Solar Fuels, an Energy Frontier Research Center funded by the U.S. Department of Energy, Office of Science, Office of Basic Energy Sciences under Award DE-SC0001011. We thank J. F. Cahoon, A. J. M. Miller, W. You, and group members for supplementary access to furnaces, reagents, and other equipment. We thank A. S. Kumbhar for

DOI: 10.1021/jacs.6b10114
J. Am. Chem. Soc. 2016, 138, 16089−16094

assistance in HR-TEM imaging. We acknowledge A. Alabanza, T. Davis, and O. Reckeweg for fruitful discussions and M. S. Druffel and L. M. Krull for proof-reading.

REFERENCES

(1) Dye, J. L. *Science* **1990**, *247*, 663.
(2) Singh, D. J.; Krakauer, H.; Haas, C.; Pickett, W. E. *Nature* **1993**, *365*, 39.
(3) Dye, J. L. *Science* **2003**, *301*, 607.
(4) Kim, S. W.; Shimoyama, T.; Hosono, H. *Science* **2011**, *333*, 71.
(5) Choi, S.; Kim, Y. J.; Kim, S. M.; Yang, J. W.; Kim, S. W.; Cho, E. J. *Nat. Commun.* **2014**, *5*, 4881.
(6) Kitano, M.; Inoue, Y.; Yamazaki, Y.; Hayashi, F.; Kanbara, S.; Matsuishi, S.; Yokoyama, T.; Kim, S.; Hara, M.; Hosono, H. *Nat. Chem.* **2012**, *4*, 934.
(7) Lu, Y.; Li, J.; Tada, T.; Toda, Y.; Ueda, S.; Yokoyama, T.; Kitano, M.; Hosono, H. *J. Am. Chem. Soc.* **2016**, *138*, 3970.
(8) Kuganathan, N.; Hosono, H.; Shluger, A. L.; Sushko, P. V. *J. Am. Chem. Soc.* **2014**, *136*, 2216.
(9) Kim, S. W.; Toda, Y.; Hayashi, K.; Hirano, M.; Hosono, H. *Chem. Mater.* **2006**, *18*, 1938.
(10) Son, Y. C.; Ryu, B.; Lee, S. M. Electrically conductive thin films. US Patent 14,567,900, December 11, 2014.
(11) Tai, P.; Jung, C.; Kang, Y.; Yoon, D. *Thin Solid Films* **2009**, *517*, 6294.
(12) Hu, J.; Xu, B.; Yang, S. A.; Guan, S.; Ouyang, C.; Yao, Y. *ACS Appl. Mater. Interfaces* **2015**, *7*, 24016.
(13) Guan, S.; Yang, S. A.; Zhu, L.; Hu, J.; Yao, Y. *Sci. Rep.* **2015**, *5*, 12285.
(14) Matsuishi, S.; Toda, Y.; Miyakawa, M.; Hayashi, K.; Kamiya, T.; Hirano, M.; Tanaka, I.; Hosono, H. *Science* **2003**, *301*, 626.
(15) Redko, M. Y.; Jackson, J. E.; Huang, R. H.; Dye, J. L. *J. Am. Chem. Soc.* **2005**, *127*, 12416.
(16) Dye, J. L.; Wagner, M. J.; Overney, G.; Huang, R. H.; Nagy, T. F.; Tomanek, D. *J. Am. Chem. Soc.* **1996**, *118*, 7329.
(17) Gregory, D. H.; Bowman, A.; Baker, C. F.; Weston, D. P. *J. Mater. Chem.* **2000**, *10*, 1635.
(18) Lee, K.; Kim, S. W.; Toda, Y.; Matsuishi, S.; Hosono, H. *Nature* **2013**, *494*, 336.
(19) Walsh, A.; Scanlon, D. O. *J. Mater. Chem. C* **2013**, *1*, 3525.
(20) Zhao, S.; Li, Z.; Yang, J. *J. Am. Chem. Soc.* **2014**, *136*, 13313.
(21) Coleman, J. N.; Lotya, M.; O'Neill, A.; Bergin, S. D.; King, P. J.; Khan, U.; Young, K.; Gaucher, A.; De, S.; Smith, R. J.; Shvets, I. V.; Arora, S. K.; Stanton, G.; Kim, H. Y.; Lee, K.; Kim, G. T.; Duesberg, G. S.; Hallam, T.; Boland, J. J.; Wang, J. J.; Donegan, J. F.; Grunlan, J. C.; Moriarty, G.; Shmeliov, A.; Nicholls, R. J.; Perkins, J. M.; Grieveson, E. M.; Theuwissen, K.; McComb, D. W.; Nellist, P. D.; Nicolosi, V. *Science* **2011**, *331*, 568.
(22) Reckeweg, O.; DiSalvo, F. J. *Solid State Sci.* **2002**, *4*, 575.
(23) Keve, E.; Skapski, A. *Chem. Commun.* **1966**, 829.
(24) Kohn, W.; Sham, L. J. *Phys. Rev.* **1965**, *140*, A1133.
(25) Hohenberg, P.; Kohn, W. *Phys. Rev.* **1964**, *136*, B864.
(26) Whittingham, M. S. Chalcogenide battery. US Patent 4009052, February 22, 1977.
(27) Aurbach, D. *J. Power Sources* **2000**, *89*, 206.
(28) Lotya, M.; Hernandez, Y.; King, P. J.; Smith, R. J.; Nicolosi, V.; Karlsson, L. S.; Blighe, F. M.; De, S.; Wang, Z.; McGovern, I. *J. Am. Chem. Soc.* **2009**, *131*, 3611.
(29) Woomer, A. H.; Farnsworth, T. W.; Hu, J.; Wells, R. A.; Donley, C. L.; Warren, S. C. *ACS Nano* **2015**, *9*, 8869.
(30) Stadelmann, P. JEMS–EMS, Java version; http://www.jems-saas.ch/.
(31) Yi, S.; Choi, J.; Lee, K.; Kim, S. W.; Park, C. H.; Cho, J. Invariance of Electronic Band Structure in Two-Dimensional Electride Materials. *arXiv preprint arXiv:1606.09347v2*, **2016**.
(32) Steinbrenner, U.; Adler, P.; Hölle, W.; Simon, A. *J. Phys. Chem. Solids* **1998**, *59*, 1527.
(33) Demri, B.; Muster, D. *J. Mater. Process. Technol.* **1995**, *55*, 311.
(34) Morris, A. J.; Nicholls, R.; Pickard, C. J.; Yates, J. *Comput. Phys. Commun.* **2014**, *185*, 1477.
(35) Pickard, C. J.; Payne, M. C. *Phys. Rev. B: Condens. Matter Mater. Phys.* **1999**, *59*, 4685.
(36) Pickard, C. J.; Payne, M. C. *Phys. Rev. B: Condens. Matter Mater. Phys.* **2000**, *62*, 4383.
(37) Oh, J. S.; Kang, C.; Kim, Y. J.; Sinn, S.; Han, M.; Chang, Y. J.; Park, B.; Kim, S. W.; Min, B. I.; Kim, H. *J. Am. Chem. Soc.* **2016**, *138*, 2496.
(38) Inoue, Y.; Kitano, M.; Kim, S.; Yokoyama, T.; Hara, M.; Hosono, H. *ACS Catal.* **2014**, *4*, 674.
(39) Rossiter, P. L. *The Electrical Resistivity of Metals and Alloys*; Cambridge University Press: Cambridge, U.K., 1991.
(40) Uijttewaal, M.; De Wijs, G.; De Groot, R. *J. Appl. Phys.* **2004**, *96*, 1751.
(41) Michaelson, H. B. *J. Appl. Phys.* **1950**, *21*, 536.

DOI: 10.1021/jacs.6b10114
J. Am. Chem. Soc. 2016, 138, 16089–16094